Available online at www.sciencedirect.com
SCIENCE DIRECT®
Journal of Nuclear Materials 349 (2006) 6–16
journal of nuclear materials
www.elsevier.com/locate/jnucmat

Deuterium depth profiling in JT-60U W-shaped divertor tiles by nuclear reaction analysis

T. Hayashi *, K. Ochiai, K. Masaki, Y. Gotoh, C. Kutsukake, T. Arai, T. Nishitani, N. Miya

Naka Fusion Research Establishment, Japan Atomic Energy Research Institute, 801 Mukouyama, Naka, Ibaraki 311-0193, Japan

Received 15 November 2004; accepted 22 June 2005

Abstract

Deuterium concentrations and depth profiles in plasma-facing graphite tiles used in the divertor of JAERI Tokamak-60 Upgrade (JT-60U) were investigated by nuclear reaction analysis (NRA). The highest deuterium concentration of $D/^{12}C$ of 0.053 was found in the outer dome wing tile, where the deuterium accumulated probably through the deuterium–carbon co-deposition. In the outer and inner divertor target tiles, the $D/^{12}C$ data were lower than 0.006. Additionally, the maximum $(H + D)/^{12}C$ in the dome top tile was estimated to be 0.023 from the results of NRA and secondary ion mass spectroscopy (SIMS). Orbit following Monte-Carlo (OFMC) simulation showed energetic deuterons caused by neutral beam injections (NBI) were implanted into the dome region with high heat flux. Furthermore, the surface temperature and conditions such as deposition and erosion significantly influenced the accumulation process of deuterium. The deuterium depth profile, scanning electron microscope (SEM) observation and OFMC simulation indicated the deuterium was considered to accumulate through three processes: the deuterium–carbon co-deposition, the implantation of energetic deuterons and the deuterium diffusion into the bulk.

PACS: 28.52.Fa; 28.52.Nh; 52.40.Hf; 52.55.Fa

1. Introduction

In a fusion tokamak reactor, tritium (T) and deuterium (D) are used as fuels of the discharge operation. Some of the tritium will be retained on the surfaces and in the bulk of the plasma-facing materials. It is one of the most important issues to evaluate the tritium inventory of in-vessel components in the present international thermal experimental reactor (ITER) design work [1]. In tokamak experimental devices, many research works regarding to plasma–wall interaction issues [2,3] and erosion/deposition issues [4] have been reported. In JT-60U, deuterium discharges have been initiated from 1991. In order to estimate the tritium retention in the future tokamak reactor including ITER, it is very important to investigate the retention characteristic of deuterium in JT-60U. After deuterium discharge period, hydrogen discharges have been performed to remove tritium from the plasma-facing wall in JT-60U. From a viewpoint of radiological problem, then, hydrogen and

* Corresponding author. Tel.: +81 29 270 7431; fax: +81 29 270 7449.
E-mail address: hayashi.takao@jaea.go.jp (T. Hayashi).

0022-3115/$ - see front matter © 2005 Published by Elsevier B.V.
doi:10.1016/j.jnucmat.2005.06.019

tritium retention of in-vessel components in JT-60U should be also evaluated.

Quite recently, qualitative analyses of deuterium and hydrogen in plasma-facing carbon tiles have been performed using SIMS [5,6]. Unfortunately, SIMS analysis presently cannot give quantitative concentrations of hydrogen isotopes such deuterium and hydrogen on the surface of the graphite tile. On the other hand, tritium distribution characteristic was investigated by tritium imaging plate technique and full combustion method, and it was clear that the tritium distribution of the JT-60U W-shaped divertor reflects mainly the distribution of the energetic triton implantation on the wall, which is produced by D–D nuclear reaction [7,8]. SEM analysis was also performed to investigate the thickness of the deposition layer on each sample tile [9].

In this study, the absolute concentrations and the depth profiles of deuterium in the graphite tiles used in the W-shaped divertor of JT-60U were investigated by NRA. The OFMC simulation of energetic deuteron caused by deuterium NBI was also performed. In addition to OFMC result, by focusing on the relationship between depth profile and surface conditions such as redeposition and erosion, deuterium accumulation processes were investigated in the study. Furthermore, the tritium distribution of the divertor region was measured by an imaging plate in order to compare with the deuterium distribution. The influence of hydrogen discharges after the deuterium operation was also examined.

2. Experimental

2.1. Sample tiles

Fig. 1(a) shows a poloidal cross section of JT-60U with the W-shaped divertor. Carbon fiber composite (CFC) material is used for the divertor plate tiles (CX-2002U), dome top tiles and a part of the baffle plate tiles (PCC-2S). All other tiles are made of isotropic graphite (IG-430U). Fig. 1(b) shows poloidal locations of analyzed samples for NRA in the W-shaped divertor region. In the toroidal direction, the sample tiles were removed from locations at the center between the toroidal magnetic field (TF) coils. In the operation period from June 1997 to October 1998, about 4300 pulse discharges experiments (~3600 deuterium discharges and ~700 hydrogen discharges) have been carried out with W-shaped divertor configurations. Inner-private flux pumping has been performed through a full toroidal inner slot. The neutral beam injections (NBI) heating with high power in the 14–23 MW range have been conducted for more than 300 discharges. During this operation period, about 1×10^{19} neutrons were produced by D–D reactions. Consequently, 1×10^{19} or 18 GBq of tritium was also produced. After deuterium discharges period, hydrogen discharges were carried out to remove the surface tritium of the carbon tiles.

Fig. 2 shows the maximum temperatures of the W-shaped divertor tiles during the deuterium discharge. The bulk temperatures were measured by thermocouples embedded in the divertor tiles at 6 mm depth. The vacuum vessel tiles were kept at constant baking temperature of about 300 °C. The high temperatures of the thermocouples were observed in plasma experiments with high power NBI heating (~20 MW), aiming at the steady-state high performance plasma discharge. The thermocouple temperatures of the inner and outer divertor tiles were relatively high. Moreover, the maximum temperatures of the outer divertor tiles (OD1–OD3) were higher than those of the inner divertor tiles (ID1–ID3). The finite element modeling analysis, which was based on bulk temperature profile in each tile and separatrix position, indicated that the temperatures of the divertor tile surfaces were expected to be 200–400 °C higher than those of the thermocouples

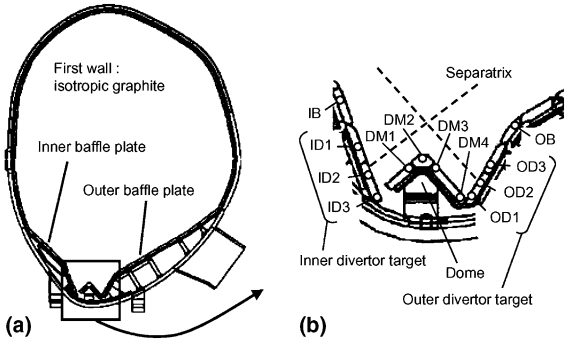

Fig. 1. (a) Poloidal cross section of JT-60U with the W-shaped divertor. (b) Twenty sample locations for NRA and a typical separatrix position in divertor region are also shown.

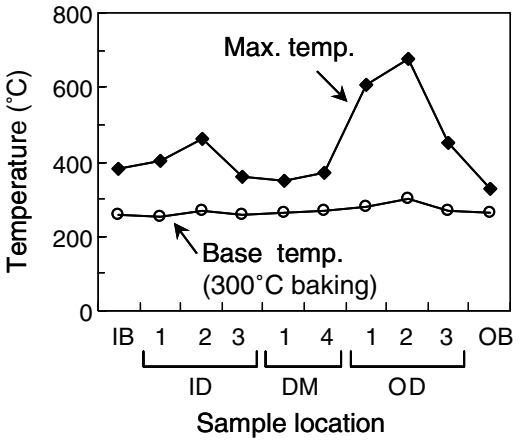

Fig. 2. Maximum temperatures of the thermocouples installed in the divertor tiles at depth of 6 mm.

shown in Fig. 2. Therefore, the highest surface temperature of the outer divertor tile is expected to be about 1100 °C [8].

2.2. Nuclear reaction analysis (NRA)

A deuterium accelerator of Fusion Neutronics Source in Japan Atomic Energy Research Institute (JAERI-FNS [10]) was used for NRA. The deuterium depth profiles in the W-shaped divertor tiles were investigated by the deuteron beam. The experimental setup for NRA is schematically shown in Fig. 3. The acceleration energy of incident deuterons was 350 keV. The incident beam of 6.5 mm diameter was adjusted to a particle current of about 0.6 μA. The finite element modeling analysis indicated that the temperature of the analyzing surface was expected to be less than the baking temperature in JT-60U (300 °C). Thus the effect of analyzing beam on the deuterium profiles is expected to be small. The amount of incident charge is directly measured from the sample with a positive bias supply of about 150 V, which is used to prevent the influence of secondary electron emission. Sample pieces, cut from the tiles to the size of 20 mm × 20 mm × 2 mm plates, were set on the movable manipulator with a sample holder in the analyzing chamber. A silicon surface-barrier detector (SBD) with 200-μm-thick silicon layer and 0.03-μm-thick Au coating layer was used to count high energetic charged particles emitted from the samples. The detector achieved energy resolution of 40 keV for 5.486 MeV α particles. The detection angle is 90°, and the solid angle for detection was 1.1×10^{-2} sr. The active area of the detector was covered with aluminum absorber foil of 6 μm thickness in order to suppress scattered deuterons. The cross-section data of D(d, p)T reaction [11] were used for determination of absolute deuterium concentrations in the samples.

Fig. 4(a) shows schematic arrangement of the analyzed sample, the silicon detector with absorber foil, and the incident deuteron beam. Fig. 4(b) shows charged-particle spectra of the dome region samples (DM1–DM4) and a fresh carbon sample, which was made from CFC material and has not been used in JT-60U. The surface-barrier detector was mounted at an angle θ_{out} of 90° relative to the incident beam. The angle θ_{in}, which denotes the angle between the incident beam and the target surface in the laboratory system, is 60°. The projected range of the deuteron beam accelerated to 350 keV is 3.0 μm. Taking into account the incident angle, the projected vertical depth from the surface in the carbon tile is 2.6 μm. Accordingly, the depth profiles by NRA were limited within 2.1 μm from the surface. In Fig. 4(a), E_{in} is the incident energy of the monoenergetic deuteron, and E_{out} is the energy of the charged particle

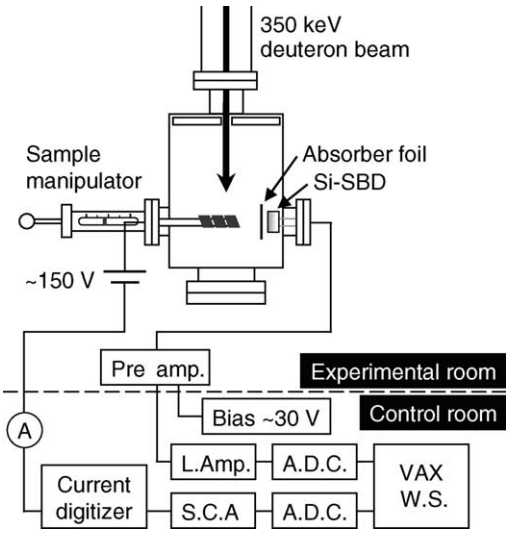

Fig. 3. Experimental setup of NRA measurement in JAERI-FNS. Conventional measurements using 350 keV deuteron beam and a silicon surface-barrier detector with aluminum absorber foil of 6 μm thickness.

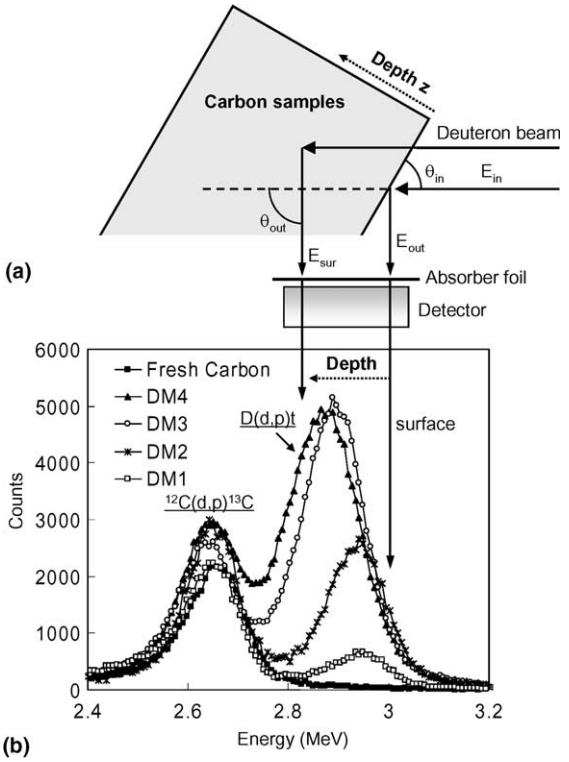

Fig. 4. (a) Schematic view of a part of experimental setup. Incident angle and detection angles are $\theta_{in} = 60°$, $\theta_{out} = 90°$, respectively. (b) Charged-particle spectra of NRA measurements. The peaks at about 2.95 MeV reflect depth profiles of deuterium.

emitted from the sample. At the sample surface, the energy E_{out} of the emitted particle is given by

$$E_{out} = k(E_{in}, \theta_{out})E_{in}, \quad (1)$$

$k(E_{in}, \theta_{out})$ is the kinematic factor. This depends on the beam energy, Q-value and the detection angle. In the case of nuclear reaction at a depth point x_1, the charged-particle energy E_{sur} at the sample surface is given by

$$E_{sur} = k(E, \theta_{out})\left\{E_{in} - \left[\frac{dE_{in}}{dx}\right]\frac{x_1}{\sin\theta_{in}}\right\} - \left[\frac{dE_{out}}{dx}\right]\frac{x_1}{\sin(\theta_{out} - \theta_{in})}, \quad (2)$$

where dE_{in}/dx and dE_{out}/dx are stopping power of the incident particle in the sample and that of the emitted particle in the sample, respectively. Ziegler's data compilation and the Stopping and Range of Ions in Matter (SRIM) code were used to estimate the stopping power in solids [12]. Because an absorber foil placed in front of the surface-barrier detector in order to suppress scattered deuterons, the emitted particle energy E_{det} at the detector surface is given by

$$E_{det} = k(E, \theta_{out})\left\{E_{in} - \left[\frac{dE_{in}}{dx}\right]\frac{x_1}{\sin\theta_{in}}\right\} - \left[\frac{dE_{out}}{dx}\right]\frac{x_1}{\sin(\theta_{out} - \theta_{in})} - \left[\frac{dE_{ab}}{dx}\right]d_1, \quad (3)$$

where dE_{ab}/dx is the stopping power of the emitted particle in absorber foil and d_1 is thickness of the absorber foil.

The yield $Y(E)$ of the nuclear reactions is given by

$$Y(E)dE = N(E)dE\left\langle\frac{d\sigma}{d\Omega}\right\rangle\Delta\Omega\phi, \quad (4)$$

where $N(E)$ is the areal concentration, $d\sigma/d\Omega$ is the differential cross section, $\Delta\Omega$ is the solid angle and ϕ is the number of incident deuteron atoms. The areal concentration depth from x to $x + \Delta x$ is described by the following equation:

$$N(x) = \frac{\int_E^{E+\Delta E} Y\,dE}{\int_x^{x+\Delta x}\left[\frac{dE_{in}}{dx}\right]dx\left\langle\frac{d\sigma}{d\Omega}\right\rangle\Delta\Omega\frac{\phi}{\sin\theta_{in}}}. \quad (5)$$

The cross section of D(d, p)T reaction can be described by the following equation [13]:

$$\sigma_{(E)} = \frac{S_{(E)}}{E}\exp\left[-31.29Z_1Z_2\left[\frac{\mu}{E}\right]^{-\frac{1}{2}}\right], \quad (6)$$

where $S_{(E)}$ is astrophysical S-factor in MeV barn. The S-factor data of D(d, p)T reaction was used the value of Ref. [14]. E is charged-particle energy in MeV, Z_1 and Z_2 are atomic number of incident and target particles, respectively, and μ is reduced mass.

In Fig. 4(b), these spectra were normalized by the number of incident deuterons, which was monitored with the current digitizer. The thick solid line shows spectrum of the fresh carbon sample. In these spectra, the peaks at about 2.95 MeV and 2.66 MeV were arised from protons due to D(d, p)T and $^{12}C(d, p)^{13}C$ reactions, respectively. In this experimental setup, the detection energy of the charged particle, emitted from D(d, p)T reaction, decreases with depth of the reaction position in the target sample. Thus the spectra show depth dependent concentrations, and the peaks at about 2.95 MeV reflect the depth profiles of the deuterium in the samples.

The energy resolution was evaluated from the peak due to $^{12}C(d, p)^{13}C$ reaction using fresh carbon sample. In the case of the nuclear reaction at the surface, the total energy resolution was 73 keV. The energy straggling of protons in aluminum foil of 6 μm thickness was 51 keV. The geometric resolution was 34 keV. Thus, the depth resolution of the NRA method using D(d, p)T reaction was 1.0 μm.

The effect of the surface roughness on the depth profile is discussed below. In order to eliminate errors caused by microscopic roughness of the order of μm or less in Rutherford backscattering spectroscopy (RBS), the incident angle between the probe beam and the target surface is required to be more than 45° [15]. The incident angle in the NRA of 60° is much larger than 45°. Assuming that the relation between incident angle and errors caused by microscopic roughness in the NRA is almost equal to that of the RBS, the influence of the surface roughness with respect to the incident particles is eliminated. Besides the emission angle, $\theta_{out} - \theta_{in}$, is 30°, which is smaller than 45°. Because the stopping power of the emission particles, in the present case, of about 20 keV/μm for 3 MeV protons in the carbon is much smaller than that of the incident beam particles of about 110 keV/μm for 350 keV deuterons, the effect of the surface roughness with respect to the emission particles is estimated to be small. From a macroscopic standpoint, because the incident beam of 6.5 mm diameter was much larger than the microscopic roughness, the influence of the roughness is averaged out.

2.3. SEM and dial gauge

In order to investigate the retention characteristic and accumulation process of deuterium, we focused on the relationship between depth profile and surface conditions such as redeposition and erosion. The net depth of erosion on the tile depends on effective tile-thickness changes, due to both areal erosion and deposition. The net depths in the eroded areas were measured by a dial gauge, and the thicknesses of redeposition layers were investigated by SEM [9]. In the SEM observation, vertical-section faces of redeposition layers on the tiles were prepared by fracturing the tiles in the poloidal direction. The thickness of redeposition layers was estimated by the differences of microstructures between base material and redeposition layer.

3. Results

3.1. Deuterium concentrations by NRA

Fig. 5(a)–(c) show deuterium depth profiles of the divertor samples: (a) the inner divertor target region, (b) the dome region, and (c) the outer divertor target region. Deuterium concentration is given by an atomic concentration ratio of deuterium to carbon ($D/^{12}C$), assuming the carbon density is 1.8 g/cm^3. It should be mentioned that the deuterium concentrations at the top surface region for all samples were very small. The main reason is that hydrogen introduced by H–H discharges replaced most of surface deuterium as discussed later, and that surface temperatures of divertor tiles were relatively high.

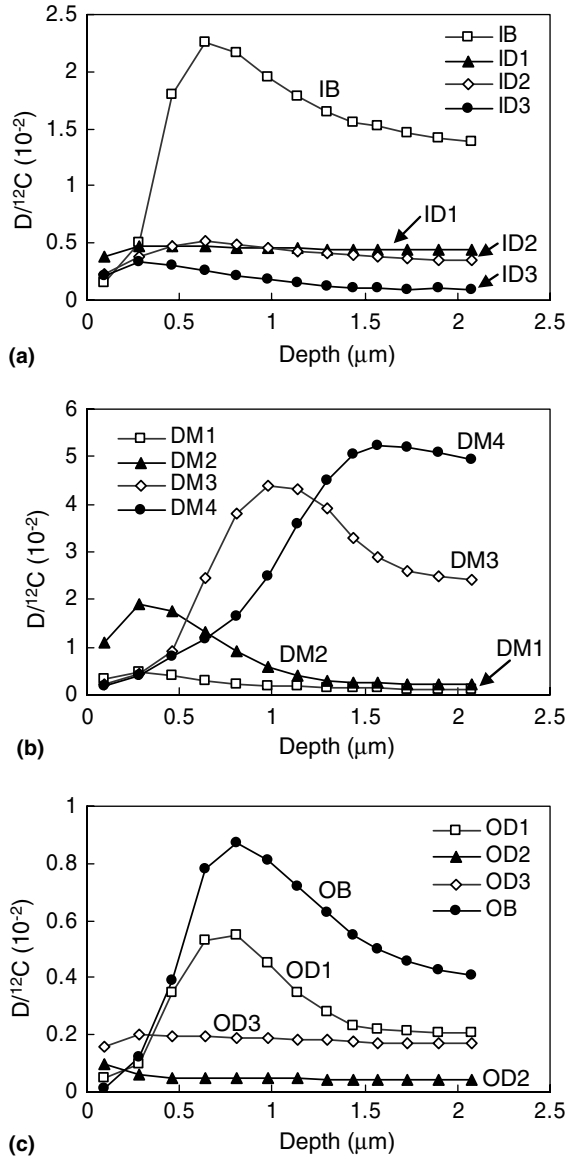

Fig. 5. Deuterium depth profiles of $D/^{12}C$ ratios in the tiles of (a) the inner divertor and baffle plate, (b) the dome unit, and (c) the outer divertor and baffle plate.

It is rather surprising to find the deuterium concentrations were very low in the inner divertor region where was deposition-dominated area (see Fig. 7). As seen in Fig. 5(a), the deuterium depth profiles of the ID1 and ID2 samples were approximately flat at $D/^{12}C$ of 0.005. And ID3, the bottom of the inner divertor tile, where no clear deposition was found, showed a little lower concentration. In Fig. 5(c), the outer divertor region except OD1 where were mostly eroded, also showed very small and flat profiles with $D/^{12}C$ of 0.0004 and 0.0019 for OD2 and OD3, respectively. Although OD1 showed a small peak at 0.8 μm, $D/^{12}C$ in the deeper area was nearly the same to that of OD3.

Compared to lower concentrations in the divertor area, the concentrations were high at both baffle plates and dome area where plasma did not directly hit. The highest deuterium concentration in the entire divertor region of JT-60U was found at the bottom of the outer dome wing tile (DM4) with the maximum $D/^{12}C$ of 0.053 at 1.6 μm depth, and keeping high concentration deep inside. Such low $D/^{12}C$ must be attributed to relatively high surface temperature of the dome tiles (~800 K). The saturation concentration of the hydrogen implanted in graphite is about 0.4–0.5 (H/C) at room temperature and decreases with temperature [16]. The H/C at 800 K is reported to be ~0.08 [16]. The difference between $D/^{12}C$ obtained by NRA and H/C in Ref. [16] is probably attributable to hydrogen introduced by H–H discharges performed after D–D discharges.

Another sample from the same outer dome wing (DM3) showed also very high concentration but a little smaller than that of DM4. The deuterium concentration in the inner dome area (DM1) was much smaller with the peak, which was much shallower than those for the outer dome wing. The maximum $D/^{12}C$ and peak position for DM2 (the dome top) and DM1 (the inner dome wing) were 0.019 at 0.3 μm, and 0.006 at 0.3 μm depth, respectively.

Fig. 6 compares the integrated deuterium amounts within 2.1 μm from the surface given in D/cm^2 and the maximum $D/^{12}C$ ratios. One can clearly see high deuterium concentration at the outer dome wing and both baffle plates.

3.2. Redeposition and erosion

Fig. 7(a)–(c) show poloidal distributions of the redeposition layer thickness and erosion depth on JT-60U divertor tiles: (a) the dome unit, (b) the inner divertor target [9], and (c) the outer divertor target [9]. In the

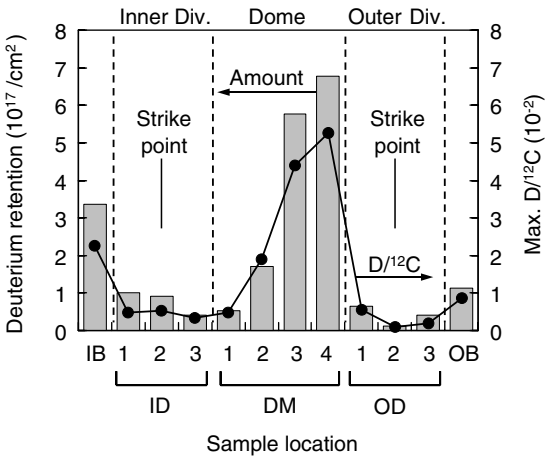

Fig. 6. Two deuterium distributions of the total amount of deuterium (D/cm^2) and of the maximum values of D/^{12}C ratios in each sample of the divertor region are shown.

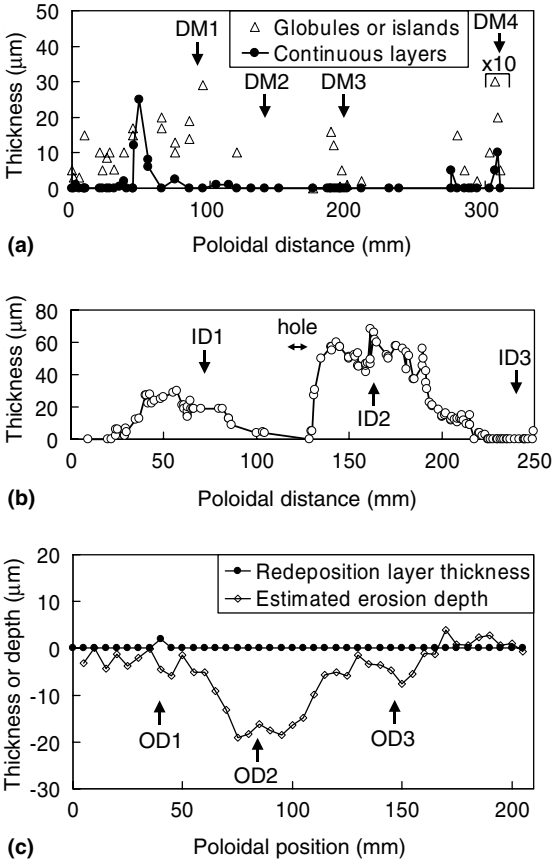

Fig. 7. Poloidal distributions of redeposition layer thickness and erosion depth on the tiles of (a) the dome unit, (b) the inner divertor, and (c) the outer divertor.

inner divertor (Fig. 7(b)), continuous redeposition layers of up to 60 μm were found on the surface. On the other hand, Fig. 7(c) indicates that erosion was more dominant than deposition in the outer divertor region, the surface of the tile was eroded to a depth of 20 μm. As shown in Fig. 7(a), the continuous layers and globular or island shaped depositions were mixed on the surface of the dome region. The NRA measurements were performed using the deuteron beam of 6.5 mm diameter (Section 2.2). Because the globular depositions were sparsely scattered on the surfaces, the influence for evaluating the deuterium concentration was relatively low. However, the continuous layer directly influenced the deuterium depth profile obtained by NRA.

3.3. Deuterium accumulation in the dome region

The highest deuterium concentrations in the whole divertor region were found in the bottom of the outer dome wing tile (DM4). The DM4 sample had maximum D/^{12}C of 0.053 at 1.6 μm depth. In typical plasma operations of JT-60U, the neutral pressure at the outer divertor region was smaller than that at the inner divertor region [17]. However, NRA results showed the deuterium concentration in the outer dome wing tile (DM3 and DM4) was higher than that of the inner dome wing (DM1). Because the continuous redeposition layers were slightly observed on the DM4 sample region, the high deuterium concentration may be attributed to the deuterium–carbon co-deposition in the DM4 region.

The deuterium depth profile of the DM4 sample had a deeper peak than the DM2 sample (Fig. 5(b)). This may be because hydrogen-containing layers were made upon the deuterium-containing layers during hydrogen discharge period. As a result, depth profile with a deep peak most likely indicates an existence of redeposition layer. Moreover, the outer dome wing tile was located facing the outer divertor target tile, which was severely eroded area. The carbon sputtered at the outer divertor tile may directly and/or indirectly accumulate as the deuterium–carbon co-deposition on the outer dome wing tile.

In the dome top tile (DM2), the deuterium depth profile had a shallower peak at 0.3 μm depth than the DM4 sample. No remarkable redeposition layer has been observed by SEM. This probably indicates that the deuterium have not accumulated as the deuterium–carbon co-deposition in the region. In deuterium plasma, the deuterium diffuses into the plasma-facing wall depending on the surface temperature, because the dome top tiles and divertor target tiles were made from CFC material. In the inner dome wing tile (DM1), SEM observation showed continuous redeposition layer was not remarkably observed on the surface (Fig. 7(a)). Thus the deuterium retention was relatively low, and the concentration decreased with the depth.

3.4. Deuterium accumulation in the inner divertor region

The redeposition was more dominant than erosion in the inner divertor region as described in Section 3.2. NRA results showed the deuterium depth profiles of the ID1 and ID2 samples were low and approximately flat at D/^{12}C of 0.005 up to depth of 2.1 μm (Fig. 5(a)). The thermocouple temperatures of the sampled positions were by 150 °C higher than the baking temperature of the vacuum vessel at 300 °C (Fig. 2), because separatrix strike positions were very close to these sample locations. In the SEM analysis, the thicknesses of redeposition layers on the ID1 and ID2 samples were ~20 μm and ~60 μm, respectively. During the experimental period, hydrogen discharges were carried out after deuterium discharges.

Considering that the analyzed depth of NRA was 2.1 μm, the hydrogen–carbon co-deposition layers, which have been deposited during the hydrogen experimental period, had a considerable influence upon the deuterium retention in the analyzed region. In the hydrogen discharge, residual deuterium gas was involved in the hydrogen–carbon co-deposition. Additionally some deuterium, which was contained in the deuterium–carbon co-deposition layer made during deuterium experimental period, might diffuse toward the surface of the hydrogen–carbon co-deposition layer due to the high temperature of the redeposition layer on the surface. Thus the low deuterium concentrations and flat depth profile were mainly caused by the hydrogen–carbon co-deposition under high temperature condition of the inner divertor target tiles (ID1 and ID2). The flat depth profiles of ID1 and ID2 were unique except for eroded region samples (OD2 and OD3) discussed in Section 3.5. The thick redeposition layers above 2 μm were only observed on the ID1 and ID2 samples. These results probably indicate that the hydrogen isotopes in the redeposition layer diffused easier than that of the base graphite. This may be attributable to that the surface temperature was much higher than that measured by thermocouples shown in Fig. 2, because the thermal conductivity of the redeposition layer might be relatively lower than base graphite.

In case of ID3 sample, the continuous redeposition layer was not remarkably observed on the surface by SEM (Fig. 7(b)). Therefore unlike in case of the ID1 and ID2 samples, the deuterium concentration decreased with the depth, because there was little influence of the redeposition layer. The deuterium depth profile showed that some deuterium in the near surface was replaced by hydrogen during hydrogen discharges.

3.5. Deuterium accumulation in the outer divertor region

The erosion was more dominant than redeposition in the outer divertor region as described in Section 3.2. NRA results showed that the deuterium concentrations were relatively low in the outer divertor region (Fig. 5(c)). The depth profiles of the OD2 and OD3 samples were approximately flat. The temperatures were considerably high in the outer divertor tiles (Fig. 2). In a dial gauge measurement, the surfaces of the OD2 and OD3 samples were eroded depth of up to 20 μm (Fig. 7(c)), because these samples were removed from the severely eroded region due to the outer separatrix touched to the outer divertor tiles. When the surface of the tile was eroded, the deuterium, which was contained in the surface region, hardly accumulated in the tile. On the other hand, the deuterium may diffuse into the pore of the graphite substrate because of the high temperature of the tile. Therefore the reasons for low deuterium concentrations and flat depth profiles were mainly the erosion of the surface, and the diffusion into the bulk under high temperature condition of the outer divertor tiles (OD2 and OD3).

In case of the OD1 sample, the erosion was not severely unlike the OD2 and OD3 samples (Fig. 7(c)). Because the continuous redeposition layers were slightly observed on the surface, the erosion was comparable with redeposition on the OD1 sample. Therefore, the erosion had little influence on the deuterium accumulation. Unlike in case of the severe eroded region (OD2 and OD3), the deuterium concentration of the OD1 sample decreased with the depth. The maximum D/^{12}C of the OD1 sample was higher than those of the OD2 and OD3 samples, and the deuterium in the near surface was replaced by hydrogen during hydrogen discharges.

4. Discussion

4.1. Hydrogen concentration by NRA and SIMS

The absolute deuterium concentrations in the subsurface layer of the carbon tiles were evaluated by NRA. Hydrogen discharges have been carried out after deuterium-discharge period to remove the tritium from the plasma-facing wall in JT-60U. Accordingly, it is very important to evaluate the hydrogen retentions in the carbon tiles. Up to now, the qualitative analyses of deuterium and hydrogen retained in carbon tiles have been performed using SIMS [5,6]. It can give only signal intensity ratios of deuterium (hydrogen) signals to carbon-12 signals (D/^{12}C and H/^{12}C). Unfortunately, this technique presently cannot give quantitative concentrations of hydrogen isotopes such as deuterium and hydrogen. In order to estimate hydrogen concentrations, we have used both the deuterium concentrations measured by NRA and the signal intensity ratios of H/^{12}C and D/^{12}C obtained by SIMS analysis. The comparison was applied to the dome top sample (DM2) in order to avoid the influence of surface conditions such as

erosion and deposition, because no severe erosion and no remarkable redeposition layer were found on the region (Section 3.2).

Fig. 8(a) shows the depth profiles of $D/^{12}C$ obtained by SIMS [5] and NRA in the dome top tile (DM2). In the figure, the ratios of SIMS analysis were normalized by the maximum signal intensity ratio of $D/^{12}C$ at 0.3 μm depth. The NRA results showed maximum $D/^{12}C$ ratio was 0.019 at 0.3 μm depth. These depth profiles of $D/^{12}C$ ratios were consistent with each other. From the results of the integral $D/^{12}C$ ($\sum D/^{12}C$) values obtained by NRA and SIMS, we can evaluate the detection efficiency of deuterium measurement in SIMS analysis. Moreover, the SIMS analysis can give the signal intensity ratios of $H/^{12}C$ as well as $D/^{12}C$. Assuming the detection efficiency of hydrogen measurement in the SIMS analysis is equal to that of deuterium measurement, we can estimate the hydrogen concentrations by both the detection efficiency and $H/^{12}C$ ratios.

From the results of NRA and SIMS, the depth profiles of $H/^{12}C$, $D/^{12}C$ and $(H + D)/^{12}C$, which was added the signal intensity ratio of $H/^{12}C$ to that of $D/^{12}C$, were obtained (Fig. 8(b)). In the very-near surface region (<0.002 μm), the $H/^{12}C$ ratio was considerably high, probably due to subsequent water adsorption when exposed to air. Except for the surface region, the $H/^{12}C$ ratios slowly decrease with depth. Comparison of the hydrogen depth profile with the deuterium depth profile showed that the deuterium in the near surface was probably replaced by hydrogen during hydrogen discharges. The maximum hydrogen isotopes concentration was estimated to be $(H + D)/^{12}C$ of 0.023 at a depth of 0.1 μm, except for surface contamination. The depth profile of $(H + D)/^{12}C$ had a shallower peak than that of $D/^{12}C$, because the hydrogen was retained in the shallower region than the deuterium. A large amount of deuterium was retained in the deep area in the dome top tile.

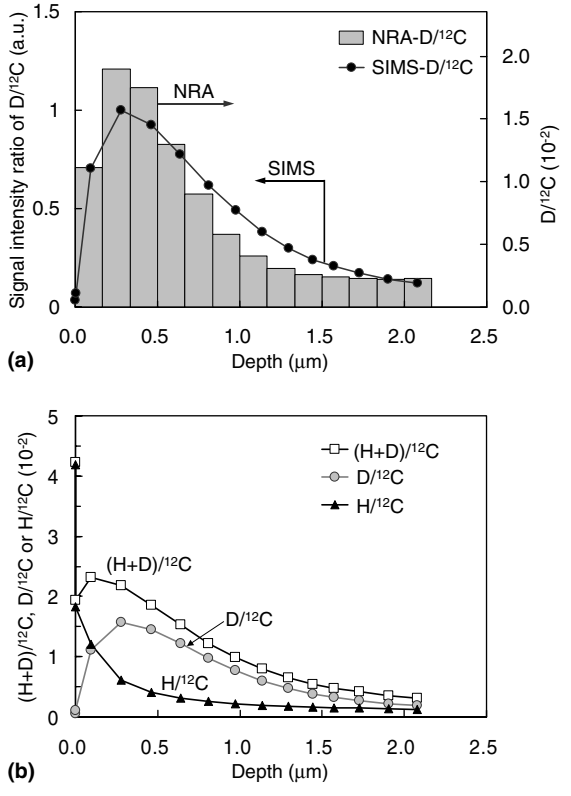

Fig. 8. In the dome top tile, (a) the depth profiles of $D/^{12}C$ measured by NRA and the signal intensity ratios of $D/^{12}C$ obtained by SIMS. (b) $H/^{12}C$, $D/^{12}C$ and $(H + D)/^{12}C$ ratios estimated by the results of NRA and SIMS.

4.2. OFMC simulation

In JT-60U, the deuterium neutral beams have been injected into deuterium plasmas. The positive-ion based neutral beam injection (PNBI) system consists of 11 beam lines, i.e., seven vertical and four tangential beam lines. The negative-ion based NBI (NNBI) system equips a tangential beam line. The incident neutral deuterium was ionized in the plasma. The energetic deuteron has been lost by ripple loss caused by the finite number of TF coils. In order to assess the energetic deuteron loss, the OFMC code [18,19] was used for a typical plasma operation of a high β_p H-mode. The ionizing points and pitch angles of deuteron test particles were determined by the Monte-Carlo method. Coulomb collisions between the energetic deuterons and the plasma were also simulated with the method. Each test particle orbit was followed until it collided with the wall or slowed down to thermal speed (~10 keV).

Fig. 9(a) shows the heat flux distribution of the energetic deuterons on the wall in a typical plasma operation of a high β_p H-mode. This figure is a 1/18 portion of the first wall cut under the TF coils. This plasma operation was performed aiming at a steady-state high performance plasma discharge in the operation period described in Section 2.1. The plasma current and toroidal field were 1.5 MA and 3.6 T, respectively. The six vertical and four tangential PNBI were injected to the plasma, which was applied to the simulation. Total NBI power was 19 MW, though NNBI was not injected to the plasma. When the neutral beam is injected, some energetic particles are lost by charge exchange. The influence of the particle loss due to the charge exchange was considered in the simulation. In Fig. 9(a), the heat flux of the outer baffle plate region was highest in the entire wall.

In the divertor region shown in Fig. 9(b), the heat flux had its maximum at the dome top tile (DM2 region) and upper part of the outer dome wing tile (DM3 region). In the toroidal direction, the heat flux was high

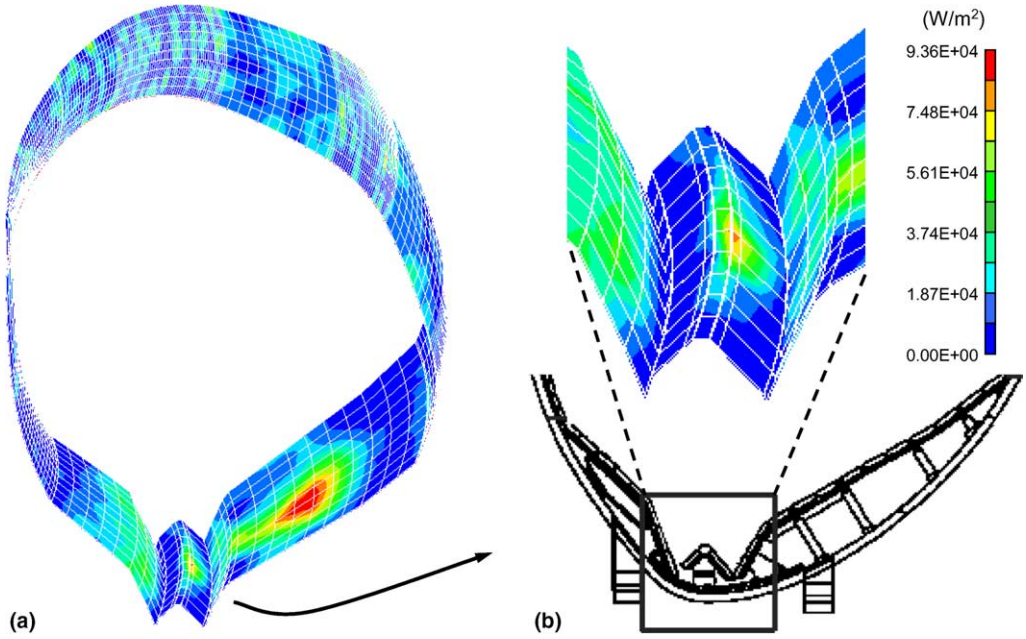

Fig. 9. The heat flux distribution of the energetic deuterons on the wall in a typical plasma operation of a high β_p H-mode, (a) at full poloidal view and (b) in the W-shaped divertor region.

at the center between the TF coils due to ripple loss. The distribution of energetic deuterons was almost consistent with that of the tritium distribution [8] in JT-60U. The OFMC simulation indicated that 0.4% of incident deuterium was implanted into the dome top region. During the discharge period from 1997 to 1998, the average energy of incident deuterium, average beam power and total incident time were 85 keV, 8 MW and 1.2×10^4 s, respectively. Considering the influence of ripple loss, the fluence and incident energy of deuteron implanted into the dome top tile (DM2 region) at the center between the TF coils was calculated to be $\sim 10^{19}$ cm^{-2} and $\sim$50 keV, respectively. The projected range of 50 keV deuteron in the carbon tile is about 0.7 μm. Compared with the peak at 0.3 μm depth of the DM2 deuterium depth profile (Fig. 5(b)), the deuterons were probably implanted at an angle. NRA showed the deuterium retention of the DM2 region was 1.7×10^{17} D/cm^2 (Section 3.1). The OFMC simulation indicated that the estimated fluence on the DM2 region was 10^{19} cm^{-2}. Under such high fluence condition, the deuterium concentration must be saturated.

In case of the DM3 sample, the deuterium depth profile had a deeper peak than the DM2 sample. This may imply that the energetic deuterons were almost vertically implanted into the DM3 region, because the setting angles of the dome top tile (DM2) and the outer dome wing tile (DM3) in the W-shaped divertor were different. The continuous redeposition layers have not been remarkably observed on both DM2 and DM3 regions by SEM. Thus, the deuterium accumulated through implantation of energetic deuteron in the dome top region (DM2 and DM3).

Because hydrogen NBI was carried out during the hydrogen discharges, the energetic proton caused by hydrogen NBI was also implanted into the DM2 and DM3 regions. The projected range of 50 keV proton in the carbon tile is about 0.5 μm, which is shorter than that of deuterium (0.7 μm). Thus the deuterium trapped in shallow area was replaced by hydrogen during hydrogen discharges. In Fig. 8(b), the deuterium and hydrogen depth profiles of the DM2 sample indicate that hydrogen was accumulated especially in surface region.

4.3. Comparison with tritium distribution

In order to compare to the deuterium distribution of the W-shaped divertor region, an imaging plate was used for measurement of the tritium distribution. Fig. 10 shows tritium and deuterium distributions on the analyzed points of NRA samples. In the figure, the tritium retentions were calibrated by that of the dome top sample (DM2), in which the highest tritium retention was recorded through the entire divertor region. The deuterium distribution differed from tritium one, especially in the dome region. The highest tritium retention was observed at the DM2 sample, while the highest deuterium retention was found at the bottom of the outer

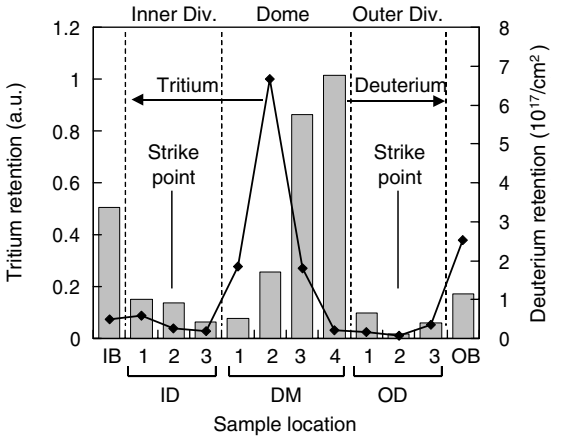

Fig. 10. Distributions of tritium and deuterium retentions on JT-60U divertor region. The tritium retentions were calibrated by that of the dome top sample (DM2), which recorded the highest tritium retention in the entire divertor region.

dome wing tile (DM4). These results indicate that the accumulation processes of the deuterium and tritium were different from each other.

The tritium distribution of the W-shaped divertor reflects mainly the distribution of the energetic triton implantation on the wall, which is produced by D–D nuclear reaction [8]. Because the deuterium gas was fed for plasma discharges in JT-60U, there were much more deuterium than tritium. Thus, the amount of tritium which accumulated through tritium–carbon deposition is much less than that of deuterium.

5. Conclusions

Quantitative concentrations and depth profiles of deuterium in the subsurface of the CFC and Graphite tiles used in the W-shaped divertor regions were investigated by NRA. The highest deuterium concentration, $D/^{12}C$ of 0.053 at 1.6 μm depth, was found at the outer dome wing tile (DM4), of which the temperature was relatively low. The deuterium depth profile and SEM observation showed that the deuterium accumulated probably through the deuterium–carbon co-deposition in the outer dome wing tile.

In the inner divertor target region (ID1 and ID2), the thick redeposition layers were observed on the surface by SEM. The deuterium concentrations of $D/^{12}C$ were lower than 0.005. The low deuterium concentrations and flat depth profiles were mainly caused by both the hydrogen–carbon co-deposition and the high temperature condition of the inner divertor target tiles. In the case of the outer divertor target region (OD2 and OD3), the surfaces of the tiles were severely eroded, and the deuterium concentrations were lower than the inner divertor tiles. The low deuterium concentration and almost flat depth profile may be caused by the erosion of the surface, and the deuterium diffusion into the bulk under considerably high temperature in the outer divertor target regions.

In the dome top tile (DM2), first quantitative estimation of hydrogen concentrations was also performed through the results of NRA and SIMS analysis. The deuterium accumulated deeper area than the hydrogen. The maximum $(H + D)/^{12}C$ was estimated to be 0.023 except for surface contamination, though the maximum $D/^{12}C$ was 0.019. According to OFMC simulation, energetic deuterons caused by NBI were implanted into the dome top region with high heat flux. Therefore, the deuterium was considered to accumulate through the implantation of energetic deuteron into the top tile (DM2) and the upper part of the outer dome wing tile (DM3).

The surface temperature and conditions such as deposition and erosion significantly influenced the accumulation process of deuterium. On the whole, in the W-shaped divertor on JT-60U, the deuterium accumulated mainly through three processes: the deuterium–carbon co-deposition, the implantation of the energetic deuteron caused by deuterium NBI and the deuterium diffusion into the bulk.

Acknowledgements

The present authors would like to express their gratitude to the operating staff of FNS. In addition, we would like to thank the JT-60 team for their contribution to the operation and the experiments of JT-60U. The first author is grateful to Dr N. Kubota for useful discussion and support.

References

[1] G. Federici, R.A. Anderl, P. Andrew, et al., J. Nucl. Mater. 266–269 (1999) 14.
[2] G. Janeschitz, ITER JCT and HTs, J. Nucl. Mater. 290–293 (2001) 1.
[3] G. Federici, C.H. Skinner, J.N. Brooks, et al., Nucl. Fusion 41 (12R) (2001) 1967.
[4] J.P. Coad, N. Bekris, J.D. Elder, et al., J. Nucl. Mater. 290–293 (2001) 224.
[5] Y. Hirohata, Y. Oya, H. Yoshida, et al., Phys. Scr. T 103 (2003) 15.
[6] Y. Oya, Y. Hirohata, Y. Morimoto, et al., J. Nucl. Mater. 313–316 (2003) 209.
[7] T. Tanabe, K. Miyasaka, K. Masaki, et al., J. Nucl. Mater. 307–311 (2002) 1441.
[8] K. Masaki, K. Sugiyama, T. Tanabe, et al., J. Nucl. Mater. 313–316 (2003) 514.

[9] Y. Gotoh, J. Yagyu, K. Masaki, et al., J. Nucl. Mater. 313–316 (2003) 370.
[10] T. Nakamura, H. Maekawa, Y. Ikeda, et al., Proc. Int. Ion Eng. Congress – ISIAT '83 & IAPT '83, Kyoto, Japan, Vol. 1, 1983, p. 567.
[11] J.W. Mayer, E. Rimini (Eds.), Ion Beam Handbook for Material Analysis, Academic Press, New York, 1977.
[12] J.F. Ziegler, Stopping Range of Ions in Matter, Pergamon, New York, 1985.
[13] C. Rolfs, E. Somorjai, Nucl. Instr. and Meth. B 99 (1995) 297.
[14] For example, <http://t2.lanl.gov/data/astro/astro.html>.
[15] Y. Itoh, T. Maeda, T. Nakajima, et al., Nucl. Instr. and Meth. B 117 (1996) 161.
[16] B.L. Doyle, W.R. Wampler, D.K. Brice, et al., J. Nucl. Mater. 103&104 (1981) 513.
[17] H. Tamai, N. Asakura, N. Hosogane, et al., J. Plasma Fusion Res. 74 (11) (1998) 1336.
[18] K. Tani, M. Azumi, H. Kishimoto, S. Tamura, J. Phys. Soc. Jpn. 50 (1981) 1726.
[19] K. Tobita, K. Tani, Y. Kusama, et al., Nucl. Fusion 35 (1995) 1585.